Kingdom of Saudi Arabia
Imam Mohammad Ibn Saud Islamic University (IMSIU)
Faculty of Sciences – Department of Physics

Studying the Radiation Shielding Properties for New Promising Saudi Cement Product as an Alternative Cementitious Material Using Geant4 Software

Thesis submitted in accordance with the requirements of
IMSIU for the degree of Bachelor in Science by

Malak Alrashed

Supervised by
Muneerah Alaqeel

IMSIU-Riyadh-KSA
February 3, 2025

Contents

List of Figures

List of Tables

Acknowledgements

I extend my heartfelt gratitude to Allah, the Almighty, for granting me the strength and guidance to complete this research successfully. I am deeply indebted to my supervisor, Dr. Muneerah Alaqeel, for her invaluable guidance, encouragement, and constructive feedback throughout this project. Her expertise and support have been instrumental in the completion of this thesis. I would also like to express my appreciation to the faculty members of the Department of Physics at Imam Muhammad Ibn Saud Islamic University for their continuous support and for providing the necessary resources to carry out this study.

Abstract

In modern construction and industrial applications, cement materials play a significant role as structural components. With the increasing demand for enhanced material properties, the radiation shielding characteristics of cementitious products have gained notable attention. This study investigates the gamma radiation shielding properties of a newly developed Saudi cement product at wide range gamma-ray and neutron energies. The `Geant4` simulation toolkit, based on the Monte Carlo statistical method, and the `eipx` software were utilized to model and analyze the interactions between these radiations and the cement material.

A wide range of gamma-ray and neutrons energies was considered to evaluate critical parameters, including the mass attenuation coefficient (μ_m) and half-value layers (HVLs). The simulated results obtained using `Geant4` were validated by comparing them with data from `eipx`, showing strong agreement within acceptable deviations. The outcomes highlight the effectiveness of the Saudi cement product as a potential alternative shielding material, particularly under high-energy gamma-ray conditions.

The dependence of μ_m and HVLs on photon energy was analyzed, revealing consistent behavior across the studied energy range. Additionally, the impact of the cement's composition on its shielding efficiency was thoroughly discussed. These findings demonstrate the promise of this new cement product for radiation protection applications in various industries.

Keywords: Geant4, eipx, neutrons, gamma radiation shielding, mass attenuation coefficient, Saudi cement, Monte Carlo simulation.

Chapter 1

Introduction

Radiation protection is a fundamental aspect of numerous applications, including medical diagnostics, nuclear energy production, and industrial processes, as radiation exposure poses significant risks. Shielding materials are therefore essential to minimize radiation exposure, ensure safety, and comply with international standards. Traditional materials such as lead and other high-density compounds have been effectively used as radiation shields due to their excellent attenuation capabilities. However, these materials are often associated with challenges related to weight, high cost, and handling difficulties. Consequently, there is increasing interest in developing alternative materials that are cost-effective, environmentally friendly, and easier to process.

Cement-based materials have emerged as a promising solution in this context. These materials are widely available, cost-effective, and possess mechanical and thermal stability, making them suitable for a range of applications. Their radiation shielding capability can be significantly enhanced by incorporating compounds such as heavy metal oxides or nanomaterials, which improve their attenuation properties. This adaptability makes cementitious compounds strong candidates for replacing traditional shielding materials, particularly in broad-scale or specialized applications.

In recent years, advancements in computational modeling have provided powerful tools for studying and improving the radiation shielding properties of materials. Simulation methods based on Monte Carlo techniques, such as Geant4, allow for precise modeling of radiation interactions with materials. Studies utilizing Geant4 have demonstrated its effectiveness in evaluating shielding properties, providing valuable insights into material performance across different energy ranges [1]. This technology enables researchers to assess material behavior under various conditions, reducing the need for costly and time-intensive experiments [2].

Previous studies have focused on the potential of cement-based materials for radiation shielding, particularly in attenuating gamma rays and neutrons [3]. A recent study investigated the low-energy gamma shielding properties of a novel Saudi cement product using Geant4. The study demonstrated the material's effectiveness within this energy range, highlighting its potential as an alternative to traditional cementitious materials [2]. However, the behavior of this material under high-energy gamma radiation and neutron exposure remains unexplored, representing a significant gap in the scientific literature.

This research aims to study the radiation shielding properties of this promising cementitious product against high-energy gamma rays and neutrons. The significance of this study lies in the growing demand for effective and sustainable shielding materials and the need to evaluate the feasibility of cement-based materials in high-energy radiation applications, which remain underexplored. Using Geant4, this research will simulate the interactions between high-energy radiation and this cementitious material, providing comprehensive insights into its radiation attenuation capabilities.

Chapter 2

Theory Concepts

2.1 Interaction of Radiation with Matter

Radiation interactions with matter are complex phenomena governed by the properties of the radiation and the medium. This chapter provides an in-depth overview of the interaction mechanisms for gamma radiation and neutrons, as well as the principles of radiation attenuation.

2.1.1 Gamma Radiation Interactions

Gamma rays interact with matter through three primary mechanisms: photoelectric absorption, Compton scattering, and pair production. The significance of each mechanism depends on the photon energy and the atomic number of the medium. Figure 2.1 illustrates the areas where each interaction dominates [4].

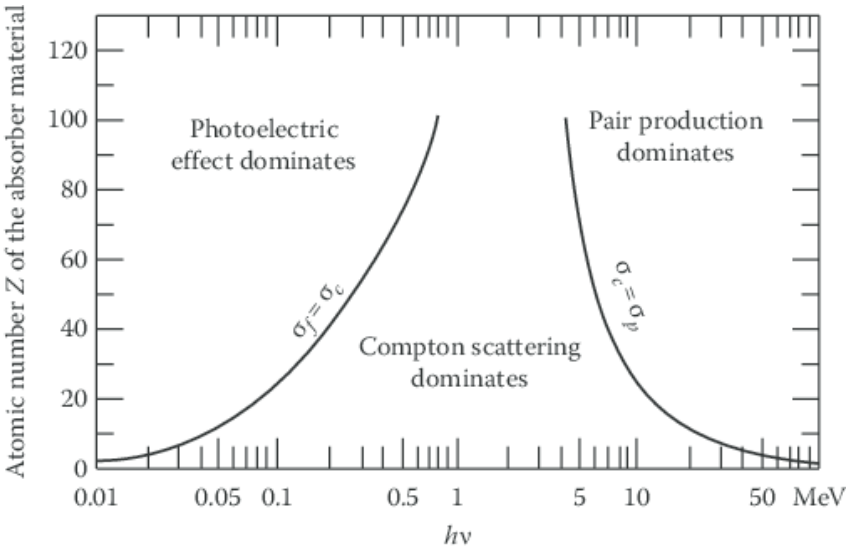

Figure 2.1: The relative importance of the three major types of gamma-ray interaction. The lines show the values of Z and $h\nu$ for which the two neighboring effects are just equal.

2.1.1.1 Photoelectric Absorption

The photoelectric effect occurs when a gamma photon is completely absorbed by an atom, resulting in the ejection of an electron from its orbital shell. This interaction can be expressed mathematically as:

$$E_\gamma = E_B + E_k, \tag{2.1}$$

where E_γ is the energy of the incoming photon, E_B is the binding energy of the electron, and E_k is the kinetic energy of the ejected electron. The cross-section for photoelectric absorption, σ_{photo}, varies approximately as:

$$\sigma_{\text{photo}} \propto Z^n E_\gamma^{-3}, \tag{2.2}$$

where Z is the atomic number, and n ranges from 4 to 5 for most elements [4]. This process dominates at low photon energies and for materials with high atomic numbers.

2.1.1.2 Compton Scattering

Compton scattering involves the interaction of a gamma photon with a loosely bound or free electron, resulting in a scattered photon and a recoiling electron. The energy and angle of the scattered photon are related by the Compton equation:

$$E' = \frac{E_\gamma}{1 + \frac{E_\gamma}{m_e c^2}(1 - \cos\theta)}, \tag{2.3}$$

where E' is the energy of the scattered photon, E_γ is the initial photon energy, m_e is the electron mass, c is the speed of light, and θ is the scattering angle. The differential cross-section is given by the Klein-Nishina formula:

$$\frac{d\sigma}{d\Omega} = \frac{r_0^2}{2}\left(\frac{1+\cos^2\theta}{[1+\alpha(1-\cos\theta)]^2}\right)\left[1 + \frac{\alpha^2(1-\cos\theta)^2}{(1+\cos^2\theta)\,[1+\alpha(1-\cos\theta)]}\right], \tag{2.4}$$

where $\alpha = \frac{h\nu}{m_e c^2}$ is the dimensionless photon energy, r_0 is the classical electron radius, and θ is the scattering angle [4].

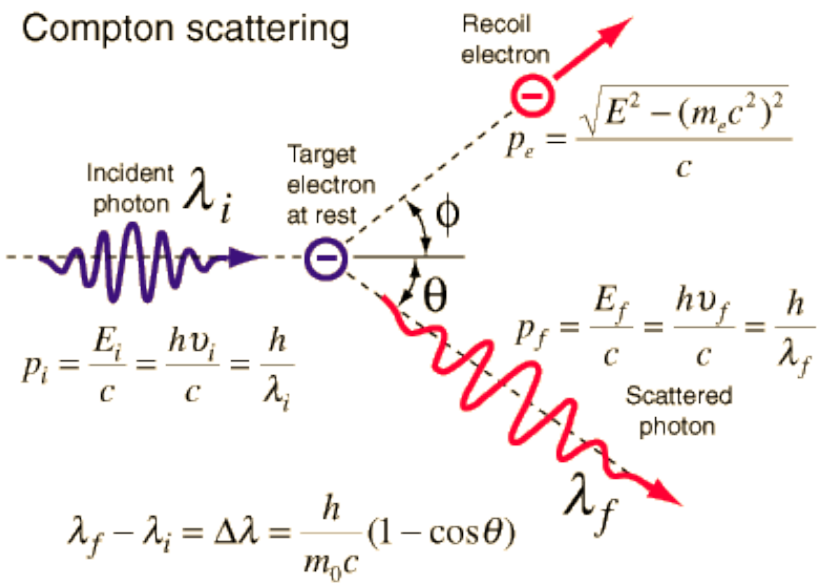

Figure 2.2: Compton Scattering

2.1.1.3 Pair Production

Pair production occurs when a gamma photon with energy exceeding 1.022 MeV interacts with the Coulomb field of a nucleus, creating an electron-positron pair. The threshold energy for this process is given by:

$$E_{\text{threshold}} = 2m_e c^2 = 1.022 \text{ MeV}. \tag{2.5}$$

The cross-section for pair production increases with photon energy and is proportional to Z^2 [4].

2.2 Interactions of Neutrons with Matter

Neutrons, alongside protons, are the fundamental constituents of atomic nuclei. Due to their lack of electric charge, neutrons interact with nuclei solely through nuclear forces. Unlike charged particles, neutrons are not impeded by a Coulomb barrier when approaching a nucleus. Consequently, the probability of nuclear interactions, quantified by the cross section, is significantly higher for neutrons than for charged particles. This section explores the characteristics of neutron interactions, focusing on cross sections and the calculation of interaction rates.

2.2.1 Types of Neutron Interactions

Neutron interactions with nuclei can be broadly classified into two categories: scattering and absorption.

2.2.1.1 Scattering

In scattering interactions, a neutron collides with a nucleus, and both particles remain present after the reaction. These reactions are typically denoted as (n, n). Scattering can occur in two forms:

- **Elastic Scattering:** In this process, the total kinetic energy of the neutron and the nucleus is conserved. The energy is redistributed between the two particles without exciting the nucleus.
- **Inelastic Scattering:** In this process, a portion of the neutron's kinetic energy is transferred to the nucleus, causing its excitation. The excited nucleus subsequently de-excites by emitting one or more gamma rays.

Scattering reactions play a crucial role in the modulation of neutrons within nuclear reactors. Neutrons produced during fission typically have an average energy of approximately 2 MeV. For these neutrons to effectively induce further fission reactions, they must slow down to "thermal" energies, typically in the eV range. This moderation is achieved through successive scattering collisions with nuclei in materials such as water or graphite [5].

2.2.1.2 Absorption

In absorption interactions, the neutron is captured by the nucleus, leading to the disappearance of the neutron and the formation of one or more new particles. Examples of absorptive reactions are summarized in Table 2.1 [5].

Table 2.1: Examples of Absorptive Neutron Reactions

Reaction	**Name**
$n + {}^{A}_{Z}X \rightarrow {}^{A-1}_{Z+1}Y + p$	(n, p) reaction
$n + {}^{A}_{Z}X \rightarrow {}^{A-4}_{Z-2}Y + \alpha$	(n, α) reaction
$n + {}^{A}_{Z}X \rightarrow {}^{A-1}_{Z}X + 2n$	$(n, 2n)$ reaction
$n + {}^{A}_{Z}X \rightarrow {}^{A}_{Z}X + \gamma$	(n, γ) reaction
$n + {}^{A}_{Z}X \rightarrow {}^{A_1}_{Z_1}Y_1 + {}^{A_2}_{Z_2}Y_2 + n + n + \ldots$	fission

2.2.2 Radiation Attenuation

Cement-based materials have emerged as a promising alternative for radiation shielding applications. Their widespread availability, cost-effectiveness, and mechanical stability make them attractive candidates for a broad range of uses. Additionally, the incorporation of heavy metal oxides, nanomaterials,

or other additives into cement can significantly enhance its attenuation properties, enabling it to compete with traditional materials in both low- and high-energy applications. This adaptability positions cementitious materials as strong contenders for replacing conventional shielding materials in specialized and large-scale projects.

The attenuation of gamma rays by a material can be described using the Beer-Lambert law:

$$I = I_0 e^{-\mu x} \tag{2.6}$$

where I is the transmitted intensity, I_0 is the initial intensity, μ is the linear attenuation coefficient, and x is the thickness of the material. For gamma radiation, the total attenuation coefficient is the sum of the coefficients for photoelectric absorption, Compton scattering, and pair production:

$$\mu = \mu_{\text{photo}} + \mu_{\text{Compton}} + \mu_{\text{pair}}. \tag{2.7}$$

The linear attenuation coefficient μ is a crucial parameter that depends on the material's composition and density. Another related parameter is the mass attenuation coefficient, defined as:

$$\mu_m = \frac{\mu}{\rho} \tag{2.8}$$

where ρ is the density of the material. The mass attenuation coefficient provides a normalized measure of a material's ability to attenuate radiation, independent of its density.

The ability of a material to attenuate gamma rays is often quantified using the half-value layer (HVL) and mean free path (MFP):

$$\text{HVL} = \frac{\ln 2}{\mu}, \quad \text{MFP} = \frac{1}{\mu} \tag{2.9}$$

HVL represents the thickness required to reduce the radiation intensity by half, while MFP describes the average distance traveled by a photon before an interaction occurs.

For neutrons, the shielding properties are characterized by the effective removal cross-section Σ_R, which represents the probability of neutron interactions per unit path length. It can be expressed as:

$$\Sigma_R = \sum_i \sigma_i N_i \tag{2.10}$$

where σ_i is the microscopic cross-section for element i, and N_i is the number density of atoms of element i in the material [4].

Recent advancements in computational modeling, particularly using Geant4's Monte Carlo simulations, have enhanced our understanding of radiation shielding materials. While previous research demonstrated the effectiveness of Saudi cement in shielding low-energy gamma rays, studies haven't thoroughly examined its performance with high-energy gamma rays and neutrons.

This research uses Geant4 to analyze a novel Saudi cementitious product's shielding capabilities across broader energy ranges, including both gamma rays and neutrons. The study aims to develop more effective radiation protection solutions by examining the material's performance in mixed radiation fields, addressing a critical gap in current shielding technology research.

The results could significantly impact applications in nuclear facilities and high-energy physics experiments, where comprehensive radiation protection is essential.

Chapter 3

Methodology

This chapter outlines the methodology used in this study to investigate the radiation shielding properties of a novel Saudi cement product using Geant4 software. The methodology involves designing the simulation environment, configuring radiation sources and detectors, and analyzing the simulation results to evaluate the material's performance under a wide range of gamma ray and neutron energies, using multiple samples for thorough evaluation.

3.1 Simulation Design

The simulation was conducted using Geant4, a Monte Carlo-based toolkit for simulating the passage of particles through matter. The simulation environment was designed to replicate realistic scenarios involving radiation interactions with the cementitious material. Five cubic samples of the Saudi cement product, each with dimensions of 10 cm x 10 cm x 10 cm, were modeled to study variations in material properties and shielding effectiveness. The physical properties of the material, including density and chemical composition, were incorporated into the simulation for accurate representation.

3.2 Radiation Sources

Two types of radiation sources were utilized in this study:

1. **Gamma rays**: The gamma radiation sources were modeled with energies ranging from 10 keV to 20 MeV, covering a comprehensive spectrum of energy levels commonly encountered in various applications.

2. **Neutrons**: Neutron sources were configured with energies ranging from 10 keV to 20 MeV, allowing for the evaluation of neutron shielding capabilities across different energy ranges.

The sources were positioned at a fixed distance of 20 cm from the sample to ensure uniform irradiation.

3.3 Physics Models

Geant4 offers a variety of physics models to simulate particle interactions. For this study, the following models were employed:

- **Electromagnetic interactions**: The Livermore and Penelope models were used for gamma ray interactions to simulate photoelectric effect, Compton scattering, and pair production.

- **Hadronic interactions**: The High Precision (HP) neutron model was applied to simulate neutron scattering, absorption, and other nuclear processes relevant to neutron attenuation.

3.4 Detector Configuration

To measure the attenuation properties of the cementitious material, virtual detectors were placed:

- **Before the sample**: To measure the initial intensity of radiation.
- **After the sample**: To measure the transmitted radiation intensity.

For each energy level, attenuation parameters such as the linear attenuation coefficient and neutron effective removal cross-sections were calculated.

3.5 Data Analysis

The simulation data were analyzed to determine the material's radiation shielding effectiveness. Key parameters included:

- **Linear attenuation coefficient (LAC)**: Quantifies the material's ability to attenuate gamma rays.
- **Neutron effective removal cross-sections**: Represents the material's capability to reduce neutron energy and flux.
- **Mean free path (MFP)**: Describes the average distance a particle travels in the material before an interaction occurs.
- **Half-value layer (HVL)**: Represents the thickness of the material required to reduce radiation intensity by half.

Data for gamma rays were compared with results obtained from EPIX simulations to evaluate the consistency and accuracy of Geant4. Neutron shielding properties were exclusively evaluated using Geant4 due to the unique nature of the neutron interactions.

3.6 Summary

This methodology provides a systematic and detailed approach for evaluating the radiation shielding properties of the Saudi cement product using Geant4. The inclusion of a wide range of energy levels, multiple samples, and a combination of gamma ray and neutron analyses ensures a comprehensive understanding of the material's shielding capabilities.

Chapter 4

Results and Discussions

4.1 Gamma Attenuation Coefficients

Five cement samples with varying chemical compositions were analyzed. The Saudi calcium bentonite sample preparation process is described in Ref. [6]. Table 4.1 presents each cement sample's conventional name, chemical structure, and density. Gamma shielding properties, including mass and linear attenuation coefficients, were determined using Geant4 simulation software. Results were compared with EpiXS theoretical calculations using Eq (4.1) in Tables 4.2 through 4.6.

$$Deviation(\%) = \frac{\mu_l(EpiXS) - \mu_l(Geant4)}{\mu_l(EpiXS)} \times 100 \tag{4.1}$$

The μ_m values for all cement samples were plotted against energies from 0.01 to 20 MeV, shown in Figs. 4.1 through 4.5.

4.1.1 Half-Value Layers

Half-Value Layer (HVL) calculations help determine effective radiation attenuators by measuring the thickness needed to reduce radiation levels by half. This metric assists radiation shielding designers in establishing safe observer distances to minimize contamination exposure. Tables 4.2 through 4.6 contain HVL values from both simulations and theoretical calculations, with percentage errors calculated using Eq (4.1).

4.1.2 Results By Sample

4.1.2.1 Sample 1

The results for this sample are presented in Fig. 4.1 and Table 4.2.

4.1.2.2 Sample 2

The results for this sample are presented in Fig. 4.2 and Table 4.3.

4.1.2.3 Sample 3

The results for this sample are presented in Fig. 4.3 and Table 4.4.

4.1.2.4 Sample 4

The results for this sample are presented in Fig. 4.4 and Table 4.5.

4.1.2.5 Sample 5

The results for this sample are presented in Fig. 4.5 and Table 4.6.

4.1.2.6 Samples Comparisons

The results of comparisons using EpiXS and Geant4 are shown in Fig 4.6.

Table 4.1: Chemical Composition and Density of the Cement Materials

Material	Chemical Oxides (wt%)										Density (g/cm^3)
	SiO_2	Al_2O_3	Fe_2O_3	CaO	MnO	K_2O	Na_2O	MgO	SO_3	TiO_2	
Sample 1: Cement	19.53	3.25	7.29	62.12	-	1.30	-	1.05	4.66	-	3.20
Sample 2: Raw Calcium Bentonite	57.98	19.70	12.46	1.11	-	1.51	1.25	1.71	-	1.62	2.47
Sample 3: Calcined Calcium Bentonite	56.63	19.86	14.89	1.16	-	1.56	1.51	1.79	-	2.20	2.59
Sample 4: Fly Ash	63.21	28.62	5.12	0.79	0.03	3.31	-	0.02	-	-	2.13
Sample 5: Silica Fume	92.72	0.70	4.81	0.81	0.31	-	-	0.49	-	-	2.41

Table 4.2: Linear Attenuation Coefficients and HVLs of Sample 1 obtained from EpiXS and Simulated by Geant4.

Energy (MeV)	EPIXS		GEANT4		% Error	
	HVL (cm)	LAC (1/cm)	HVL (cm)	LAC (1/cm)	HVL	LAC
0.01	0.00371861	186.399	0.003784	183.16	-1.76	1.74
0.02	0.026345	26.3104	0.026466	26.19008	-0.46	0.46
0.03	0.0826397	8.38758	0.083097	8.341472	-0.55	0.55
0.04	0.178409	3.88517	0.181798	3.812736	-1.90	1.86
0.05	0.307578	2.25356	0.313586	2.21039	-1.95	1.92
0.06	0.455639	1.52126	0.458545	1.511622	-0.64	0.63
0.081	0.765198	0.905841	0.771458	0.89849	-0.82	0.81
0.112	1.11943	0.619198	1.130224	0.613283	-0.96	0.96
0.122	1.2057	0.574894	1.218949	0.568643	-1.10	1.09
0.136	1.3113	0.528597	1.328039	0.521933	-1.28	1.26
0.161	1.46319	0.473723	1.484718	0.466854	-1.47	1.45
0.223	1.73651	0.399162	1.76136	0.39353	-1.43	1.41
0.276	1.91213	0.362501	1.935335	0.358154	-1.21	1.20
0.302	1.98784	0.348694	2.010288	0.3448	-1.13	1.12
0.356	2.13607	0.324496	2.152182	0.322067	-0.75	0.75
0.384	2.20472	0.314392	2.220523	0.312155	-0.72	0.71
0.511	2.49685	0.277609	2.503351	0.276888	-0.26	0.26
0.662	2.80587	0.247035	2.805777	0.247043	0.00	0.00
0.835	3.12787	0.221604	3.120935	0.222096	0.22	-0.22
0.84	3.13725	0.220941	3.12971	0.221473	0.24	-0.24
1.17	3.69437	0.187622	3.711681	0.186748	-0.47	0.47
1.275	3.85783	0.179673	3.875226	0.178866	-0.45	0.45
1.333	3.94878	0.175534	3.95961	0.175054	-0.27	0.27
2	4.84529	0.143056	4.875155	0.14218	-0.62	0.61
3	5.88033	0.117875	5.940469	0.116682	-1.02	1.01
5	7.23747	0.095772	7.317558	0.094724	-1.11	1.09
6	7.67585	0.0903023	7.761409	0.089307	-1.11	1.10
8	8.25722	0.0839443	8.350913	0.083003	-1.13	1.12
10	8.5897	0.0807011	8.687901	0.079783	-1.14	1.14
20	8.89953	0.0778859	8.998695	0.077028	-1.11	1.10

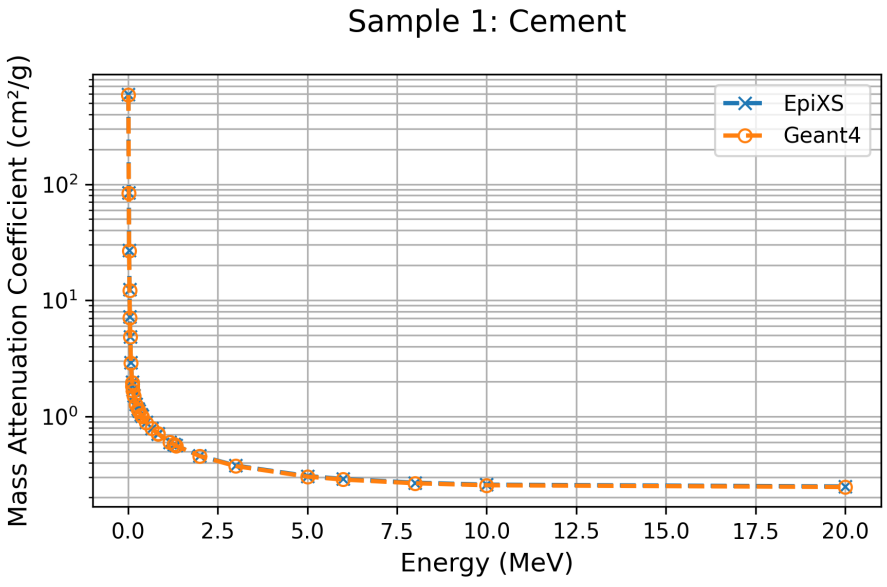

Figure 4.1: μ_m comparison for Sample 1 between EpiXS data and simulated Geant4 data.

Table 4.3: Linear Attenuation Coefficients and HVLs of Sample 2 obtained from EpiXS and Simulated by Geant4.

Energy (MeV)	EPIXS		GEANT4		% Error	
	HVL (cm)	LAC (1/cm)	HVL (cm)	LAC (1/cm)	HVL	LAC
0.01	0.00835576	82.9544	0.009039	76.680162	-8.18	7.56
0.02	0.0586762	11.8131	0.062705	11.05404	-6.87	6.43
0.03	0.177784	3.89882	0.188363	3.679855	-5.95	5.62
0.04	0.363703	1.9058	0.386566	1.793087	-6.29	5.91
0.05	0.588583	1.17765	0.622923	1.112733	-5.83	5.51
0.06	0.817636	0.847718	0.852069	0.813487	-4.21	4.04
0.081	1.22749	0.564688	1.273548	0.544265	-3.75	3.62
0.112	1.63099	0.424986	1.687248	0.410815	-3.45	3.33
0.122	1.72403	0.40205	1.783782	0.388583	-3.47	3.35
0.136	1.8383	0.37706	1.901856	0.364458	-3.46	3.34
0.161	2.00452	0.345791	2.074381	0.334147	-3.49	3.37
0.223	2.3185	0.298964	2.393096	0.289645	-3.22	3.12
0.276	2.53054	0.273913	2.605098	0.266073	-2.95	2.86
0.302	2.62405	0.264151	2.698772	0.256838	-2.85	2.77
0.356	2.81008	0.246664	2.878898	0.240768	-2.45	2.39
0.384	2.89687	0.239274	2.966659	0.233646	-2.41	2.35
0.511	3.27084	0.211917	3.334265	0.207886	-1.94	1.90
0.662	3.66992	0.188873	3.731481	0.185757	-1.68	1.65
0.835	4.08778	0.169566	4.147155	0.167138	-1.45	1.43
0.84	4.09998	0.169061	4.158746	0.166672	-1.43	1.41
1.17	4.82508	0.143655	4.92941	0.140615	-2.16	2.12
1.275	5.03876	0.137563	5.146936	0.134672	-2.15	2.10
1.333	5.15789	0.134386	5.25946	0.131791	-1.97	1.93
2	6.3489	0.109176	6.497907	0.106672	-2.35	2.29
3	7.77321	0.0891713	7.994439	0.086704	-2.85	2.77
5	9.76897	0.070954	10.075809	0.068793	-3.14	3.05
6	10.4664	0.0662257	10.805791	0.064146	-3.24	3.14
8	11.4671	0.0604466	11.859591	0.058446	-3.42	3.31
10	12.113	0.0572236	12.54583	0.055249	-3.57	3.45
20	13.1441	0.0527344	13.67042	0.050704	-4.00	3.85

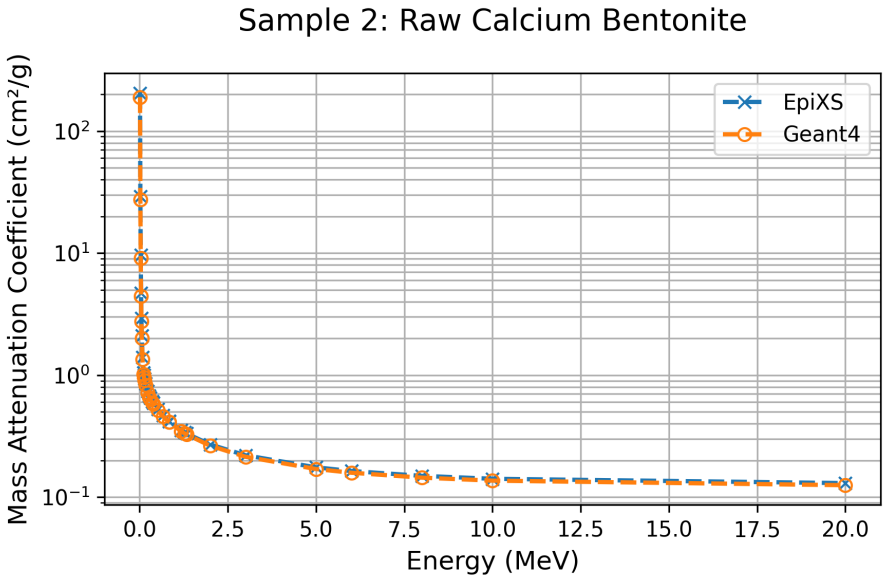

Figure 4.2: μ_m comparison for Sample 2 between EpiXS data and simulated Geant4 data.

Table 4.4: Linear Attenuation Coefficients and HVLs of Sample 3 obtained from EpiXS and Simulated by Geant4.

Energy (MeV)	EPIXS		GEANT4		% Error	
	HVL (cm)	LAC (1/cm)	HVL (cm)	LAC (1/cm)	HVL	LAC
0.01	0.00742218	93.3887	0.007815	88.697658	-5.29	5.02
0.02	0.0518498	13.3684	0.053924	12.854196	-4.00	3.85
0.03	0.157599	4.39816	0.162643	4.261767	-3.20	3.10
0.04	0.324994	2.1328	0.336993	2.056861	-3.69	3.56
0.05	0.531382	1.30442	0.549205	1.262091	-3.35	3.25
0.06	0.745844	0.929346	0.758983	0.913257	-1.76	1.73
0.081	1.13912	0.608494	1.154763	0.600251	-1.37	1.35
0.112	1.53468	0.451655	1.55114	0.446863	-1.07	1.06
0.122	1.62644	0.426174	1.644198	0.421572	-1.09	1.08
0.136	1.73891	0.398609	1.757923	0.394299	-1.09	1.08
0.161	1.90207	0.364418	1.923501	0.360357	-1.13	1.11
0.223	2.20751	0.313995	2.226882	0.311264	-0.88	0.87
0.276	2.41213	0.287359	2.42697	0.285602	-0.62	0.61
0.302	2.50209	0.277027	2.515054	0.275599	-0.52	0.52
0.356	2.68065	0.258574	2.6841	0.258242	-0.13	0.13
0.384	2.76386	0.250789	2.766338	0.250565	-0.09	0.09
0.511	3.12182	0.222033	3.11027	0.222858	0.37	-0.37
0.662	3.50339	0.19785	3.48142	0.199099	0.63	-0.63
0.835	3.90267	0.177608	3.869613	0.179126	0.85	-0.85
0.84	3.91433	0.177079	3.880431	0.178626	0.87	-0.87
1.17	4.60695	0.150457	4.599827	0.15069	0.15	-0.15
1.275	4.81097	0.144077	4.802807	0.144321	0.17	-0.17
1.333	4.92469	0.140749	4.907784	0.141234	0.34	-0.34
2	6.06046	0.114372	6.061969	0.114344	-0.02	0.02
3	7.41509	0.0934779	7.453016	0.093002	-0.51	0.51
5	9.30403	0.0744996	9.378187	0.073911	-0.80	0.79
6	9.96049	0.0695897	10.049658	0.068972	-0.90	0.89
8	10.8972	0.063608	11.013848	0.062934	-1.07	1.06
10	11.4969	0.06029	11.636855	0.059565	-1.22	1.20
20	12.4286	0.0557705	12.631419	0.054875	-1.63	1.61

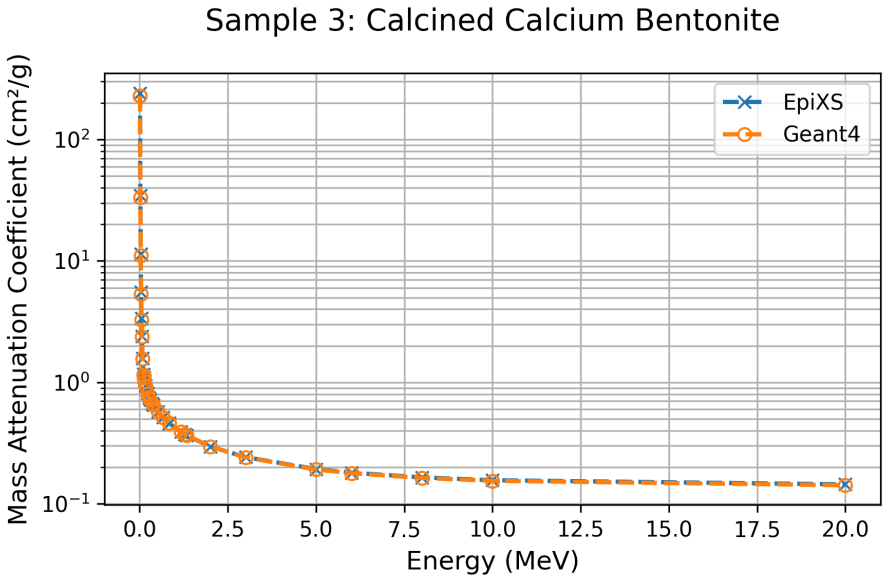

Figure 4.3: μ_m comparison for Sample 3 between EpiXS data and simulated Geant4 data.

Table 4.5: Linear Attenuation Coefficients and HVLs of Sample 4 obtained from EpiXS and Simulated by Geant4.

Energy (MeV)	EPIXS		GEANT4		% Error	
	HVL (cm)	LAC (1/cm)	HVL (cm)	LAC (1/cm)	HVL	LAC
0.01	0.0127611	54.3172	0.013883	49.928052	-8.79	8.08
0.02	0.0920785	7.52779	0.09887	7.010725	-7.38	6.87
0.03	0.275123	2.51941	0.290607	2.385174	-5.63	5.33
0.04	0.542771	1.27705	0.568547	1.219154	-4.75	4.53
0.05	0.839595	0.825573	0.868659	0.797951	-3.46	3.35
0.06	1.11745	0.620292	1.134718	0.610854	-1.55	1.52
0.081	1.56864	0.441878	1.575333	0.44	-0.43	0.43
0.112	1.98227	0.349674	1.979496	0.350163	0.14	-0.14
0.122	2.07649	0.333808	2.072694	0.334419	0.18	-0.18
0.136	2.19359	0.315987	2.187676	0.316842	0.27	-0.27
0.161	2.3667	0.292875	2.359031	0.293827	0.32	-0.33
0.223	2.7062	0.256129	2.68781	0.257885	0.68	-0.69
0.276	2.9426	0.235556	2.914107	0.237859	0.97	-0.98
0.302	3.04804	0.227408	3.015421	0.229867	1.07	-1.08
0.356	3.25937	0.212663	3.211753	0.215816	1.46	-1.48
0.384	3.35836	0.206394	3.307926	0.209541	1.50	-1.52
0.511	3.78726	0.183021	3.713031	0.18668	1.96	-2.00
0.662	4.24668	0.163221	4.152815	0.16691	2.21	-2.26
0.835	4.72868	0.146584	4.613417	0.150246	2.44	-2.50
0.84	4.74277	0.146148	4.626752	0.149813	2.45	-2.51
1.17	5.58018	0.124216	5.482865	0.126421	1.74	-1.78
1.275	5.82727	0.118949	5.724832	0.121077	1.76	-1.79
1.333	5.9651	0.1162	5.85009	0.118485	1.93	-1.97
2	7.34776	0.0943345	7.233978	0.095818	1.55	-1.57
3	9.01492	0.0768889	8.922029	0.077689	1.03	-1.04
5	11.3861	0.0608764	11.312074	0.061275	0.65	-0.65
6	12.2291	0.05668	12.167144	0.056969	0.51	-0.51
8	13.4589	0.0515012	13.4253	0.05163	0.25	-0.25
10	14.2727	0.048567	14.267416	0.048583	0.04	-0.03
20	15.6751	0.0442196	15.773792	0.043943	-0.63	0.63

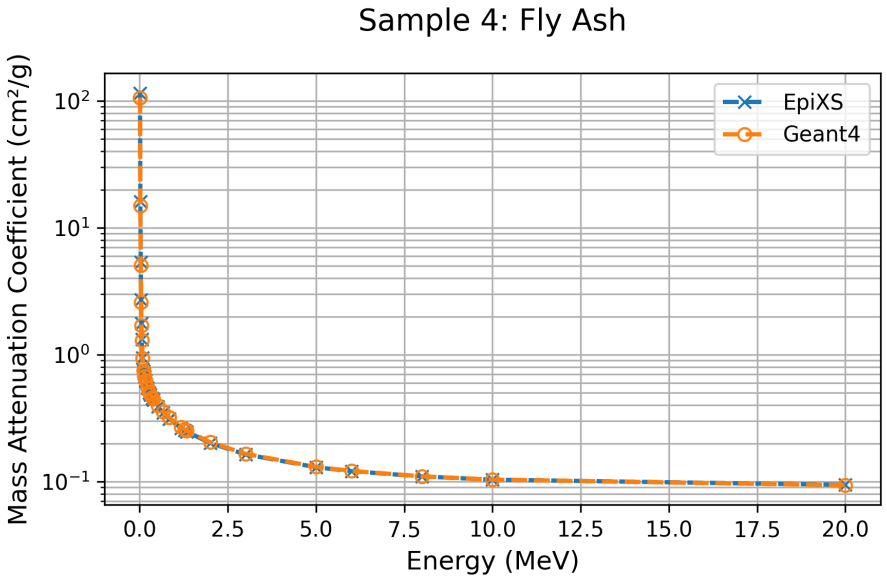

Figure 4.4: μ_m comparison for Sample 4 between EpiXS data and simulated Geant4 data.

Table 4.6: Linear Attenuation Coefficients and HVLs of Sample 5 obtained from EpiXS and Simulated by Geant4.

Energy (MeV)	EPIXS		GEANT4		% Error	
	HVL (cm)	LAC (1/cm)	HVL (cm)	LAC (1/cm)	HVL	LAC
0.01	0.0116886	59.3011	0.011756	58.959204	-0.58	0.58
0.02	0.0844089	8.21178	0.084546	8.198507	-0.16	0.16
0.03	0.251291	2.75834	0.250198	2.770391	0.43	-0.44
0.04	0.492704	1.40682	0.492227	1.408187	0.10	-0.10
0.05	0.757171	0.915444	0.757081	0.915552	0.01	-0.01
0.06	1.00168	0.691983	0.995914	0.695991	0.58	-0.58
0.081	1.39448	0.497066	1.394413	0.497089	0.00	0.00
0.112	1.75181	0.395675	1.761449	0.39351	-0.55	0.55
0.122	1.83325	0.378098	1.845648	0.375558	-0.68	0.67
0.136	1.93474	0.358264	1.949244	0.355598	-0.75	0.74
0.161	2.08497	0.332449	2.103987	0.329445	-0.91	0.90
0.223	2.38111	0.291102	2.399814	0.288834	-0.79	0.78
0.276	2.58807	0.267824	2.602808	0.266307	-0.57	0.57
0.302	2.68046	0.258593	2.693585	0.257333	-0.49	0.49
0.356	2.86587	0.241863	2.869386	0.241566	-0.12	0.12
0.384	2.95275	0.234746	2.955469	0.23453	-0.09	0.09
0.511	3.3294	0.20819	3.317855	0.208914	0.35	-0.35
0.662	3.73301	0.185681	3.711072	0.186778	0.59	-0.59
0.835	4.15659	0.166759	4.123258	0.168107	0.80	-0.81
0.84	4.16897	0.166263	4.134752	0.167639	0.82	-0.83
1.17	4.90493	0.141316	4.899935	0.14146	0.10	-0.10
1.275	5.12214	0.135324	5.11612	0.135483	0.12	-0.12
1.333	5.24331	0.132196	5.228005	0.132583	0.29	-0.29
2	6.45965	0.107304	6.462573	0.107256	-0.05	0.04
3	7.92875	0.087422	7.962993	0.087046	-0.43	0.43
5	10.0247	0.0691437	10.07235	0.068817	-0.48	0.47
6	10.7727	0.064343	10.821059	0.064055	-0.45	0.45
8	11.8676	0.0584068	11.914224	0.058178	-0.39	0.39
10	12.5949	0.0550339	12.637994	0.054846	-0.34	0.34
20	13.8701	0.0499744	13.888977	0.049906	-0.14	0.14

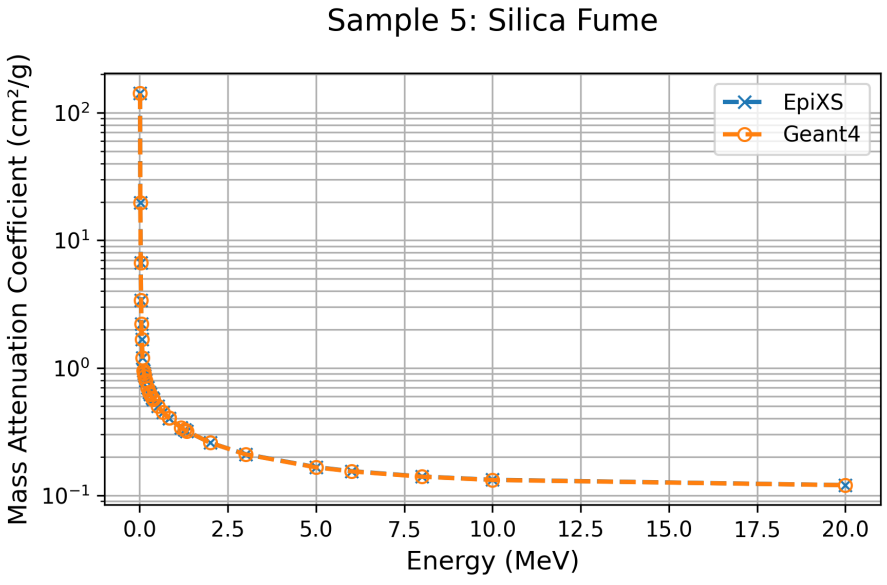

Figure 4.5: μ_m comparison for Sample 5 between EpiXS data and simulated Geant4 data.

4.1.3 Results Summary

The simulation results demonstrated a well-defined attenuation capability for gamma radiation across all evaluated cement-based samples over a wide energy range. The obtained results aligned with the theoretical values from EpiXS with a deviation of less than 10%.

Sample 5, which contained silica fume, exhibited the highest gamma-ray attenuation strength, with minimal variation of less than 1% among the tested cementitious compounds. This behavior can be attributed to the crystalline nature of silica, which enhances the scattering of gamma rays.

The fly ash cement sample, which ranked second after silica fume, displayed superior attenuation properties compared to the two bentonite-based composites. The promising Saudi calcium bentonite-based cement exhibited competitive shielding characteristics, making it a potential candidate for radiation shielding applications.

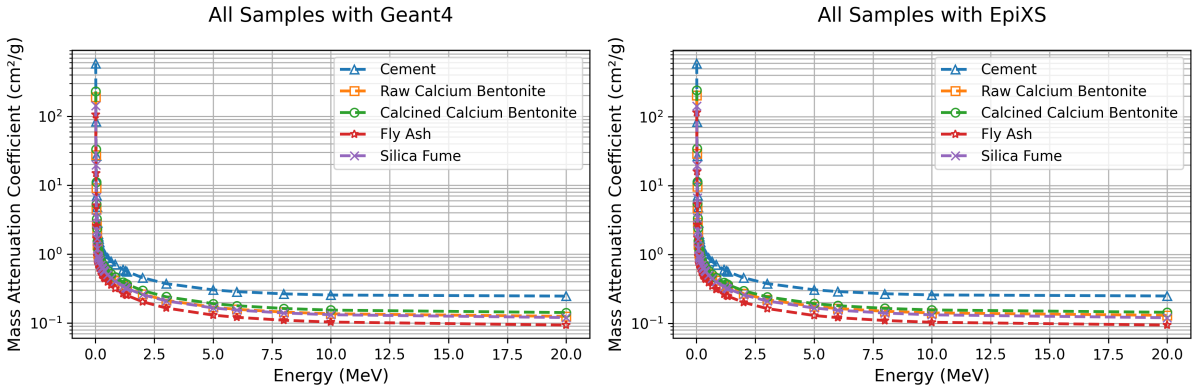

Figure 4.6: μ_m comparison for all five samples simulated using Geant4 and EpiXS, respectively.

4.2 Neutron Results

Neutron shielding properties, including mass and linear attenuation coefficients, were determined using Geant4 simulation software. Results are shown in Tables 4.7 through 4.11. The μ_m values for all cement samples were plotted against energies from 0.01 to 20 MeV, shown in Figs. 4.7 through 4.11.

4.2.1 Results By Sample

4.2.1.1 Sample 1

The results for this sample are presented in Fig. 4.7 and Table 4.7.

4.2.1.2 Sample 2

The results for this sample are presented in Fig. 4.8 and Table 4.8.

4.2.1.3 Sample 3

The results for this sample are presented in Fig. 4.9 and Table 4.9.

4.2.1.4 Sample 4

The results for this sample are presented in Fig. 4.10 and Table 4.10.

4.2.1.5 Sample 5

The results for this sample are presented in Fig. 4.11 and Table 4.11.

4.2.1.6 Samples Comparisons

The results of comparisons using Geant4 simulations are shown in Fig 4.12.

Table 4.7: Results for Sample 1 obtained from Geant4 simulation.

Energy (MeV)	Geant4			
	Mass Attenuation Coefficient (cm^2/g)	LAC (1/cm)	HVL (cm)	MFP (cm)
0.01	7.254	23.2128	0.02986056	0.04307968
0.02	6.5668	21.01376	0.0329854	0.04758787
0.03	7.5638	24.20416	0.02863752	0.04131521
0.04	6.424	20.5568	0.03371863	0.0486457
0.05	6.2061	19.85952	0.03490251	0.05035368
0.06	6.4995	20.7984	0.03332695	0.04808062
0.081	3.3988	10.87616	0.06373087	0.09194422
0.112	7.3198	23.42336	0.02959213	0.04269242
0.122	6.0392	19.32544	0.03586708	0.05174526
0.136	7.6803	24.57696	0.02820313	0.04068851
0.161	14.869	47.5808	0.01456779	0.02101688
0.223	15.475	49.52	0.01399732	0.02019386
0.276	7.7143	24.68576	0.02807883	0.04050918
0.302	6.6499	21.27968	0.0325732	0.04699319
0.356	12.798	40.9536	0.01692518	0.02441788
0.384	8.7384	27.96288	0.02478812	0.0357617
0.511	9.4893	30.36576	0.0228266	0.03293183
0.662	6.1738	19.75616	0.03508512	0.05061712
0.835	5.4759	17.52288	0.03955669	0.05706824
0.84	5.4965	17.5888	0.03940844	0.05685436
1.17	6.2739	20.07648	0.03452533	0.04980953
1.275	6.0864	19.47648	0.03558893	0.05134398
1.333	10.544	33.7408	0.02054329	0.02963771
2	4.4824	14.34368	0.04832422	0.06971712
3	4.9408	15.81056	0.04384077	0.06324887
5	4.5923	14.69536	0.04716776	0.06804869
6	4.9784	15.93088	0.04350966	0.06277117
8	3.7679	12.05728	0.05748786	0.08293745
10	4.2295	13.5344	0.05121374	0.0738858
20	4.2654	13.64928	0.05078269	0.07326394

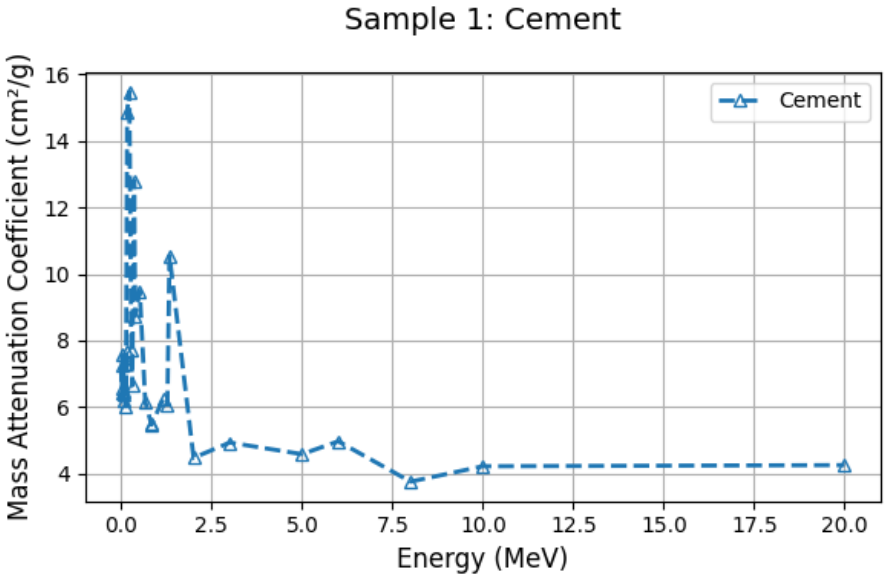

Figure 4.7: μ_m for Sample 1 simulated using Geant4.

Table 4.8: Results for Sample 2 obtained from Geant4 simulation.

Energy (MeV)	Geant4			
	Mass Attenuation Coefficient (cm^2/g)	LAC (1/cm)	HVL (cm)	MFP (cm)
0.01	9.9334	24.535498	0.02825079	0.04075727
0.02	10.198	25.18906	0.02751779	0.03969977
0.03	11.045	27.28115	0.02540755	0.03665535
0.04	9.3358	23.059426	0.03005917	0.04336621
0.05	8.6832	21.447504	0.03231831	0.04662547
0.06	10.027	24.76669	0.02798707	0.04037681
0.081	9.6552	23.848344	0.02906479	0.04193163
0.112	8.3108	20.527676	0.03376647	0.04871472
0.122	7.9879	19.730113	0.03513143	0.05068395
0.136	7.659	18.91773	0.03664008	0.05286046
0.161	8.4344	20.832968	0.03327165	0.04800084
0.223	12.157	30.02779	0.02308352	0.03330248
0.276	10.012	24.72964	0.028029	0.04043731
0.302	9.7474	24.076078	0.02878987	0.041535
0.356	10.09	24.9223	0.02781233	0.04012471
0.384	12.078	29.83266	0.02323451	0.03352031
0.511	11.233	27.74551	0.02498232	0.03604187
0.662	8.4063	27.74551	0.03338287	0.0481613
0.835	9.5502	20.763561	0.02938435	0.04239265
0.84	9.4678	23.588994	0.02964008	0.0427616
1.17	7.8166	19.307002	0.03590134	0.05179468
1.275	9.0246	22.290762	0.03109571	0.04486163
1.333	11.782	29.10154	0.02381823	0.03436244
2	5.7192	14.126424	0.04906742	0.07078932
3	4.4859	11.080173	0.06255743	0.0902513
5	4.3673	10.787231	0.06425627	0.0927022
6	5.0414	12.452258	0.05566438	0.08030672
8	3.7279	9.207913	0.07527734	0.10860224
10	4.3438	10.729186	0.06460389	0.09320372
20	4.8821	12.058787	0.05748067	0.08292708

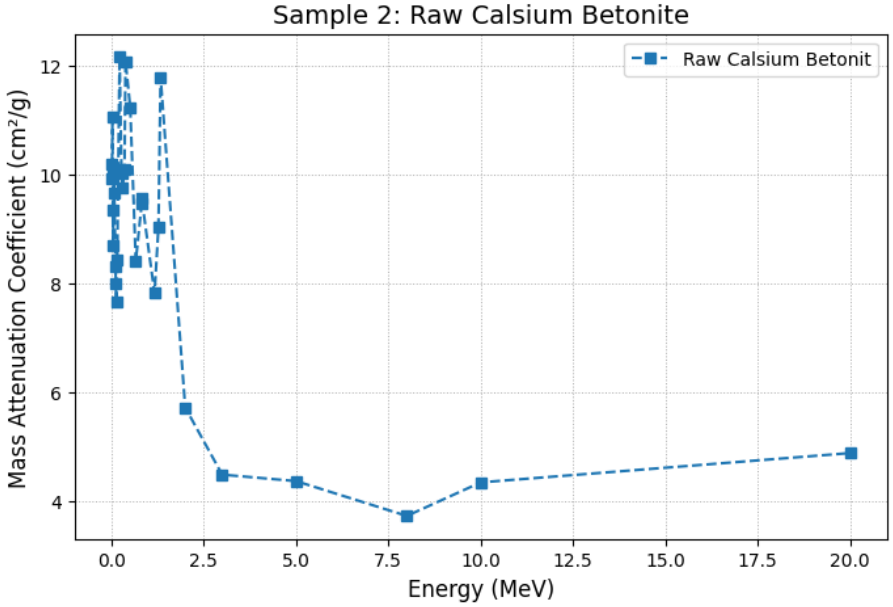

Figure 4.8: μ_m for Sample 2 simulated using Geant4.

Table 4.9: Results for Sample 3 obtained from Geant4 simulation.

Energy (MeV)	Geant4			
	Mass Attenuation Coefficient (cm^2/g)	LAC (1/cm)	HVL (cm)	MFP (cm)
0.01	10.253	26.55527	0.02610206	0.03765731
0.02	10.688	27.68192	0.02503971	0.03612466
0.03	11.598	30.03882	0.02307505	0.03329026
0.04	9.5577	24.754443	0.02800092	0.04039679
0.05	8.8719	22.978221	0.0301654	0.04351947
0.06	10.21	26.4439	0.02621199	0.0378159
0.081	9.8157	25.422663	0.02726493	0.03933498
0.112	8.4647	21.923573	0.03161652	0.045613
0.122	8.1252	21.044268	0.03293758	0.04751888
0.136	7.777	20.14243	0.03441229	0.04964644
0.161	8.5646	22.182314	0.03124774	0.04508096
0.223	12.263	31.76117	0.02182373	0.03148499
0.276	10.373	26.86607	0.0258001	0.03722167
0.302	9.8184	25.429656	0.02725743	0.03932417
0.356	10.176	26.35584	0.02629957	0.03794225
0.384	12.26	31.7534	0.02182907	0.03149269
0.511	11.374	29.45866	0.02352949	0.03394588
0.662	8.49	21.9891	0.03152231	0.04547708
0.835	9.6117	24.894303	0.02784361	0.04016983
0.84	9.5577	24.754443	0.02800092	0.04039679
1.17	7.9199	20.512541	0.03379139	0.04875066
1.275	9.1244	23.632196	0.02933063	0.04231515
1.333	11.924	30.88316	0.02244418	0.03238011
2	5.7966	15.013194	0.0461692	0.06660808
3	4.5751	11.849509	0.05849586	0.08439168
5	4.4501	11.525759	0.06013896	0.08676218
6	5.1402	13.313118	0.05206498	0.07511388
8	3.8065	9.858835	0.07030721	0.10143186
10	4.4258	11.462822	0.06046916	0.08723855
20	4.9531	12.828529	0.0540317	0.07795126

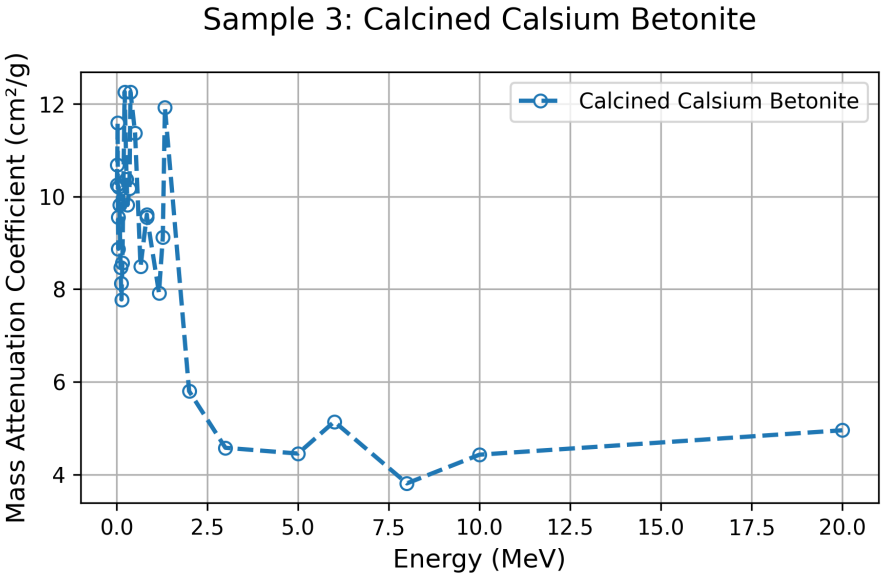

Figure 4.9: μ_m for Sample 3 simulated using Geant4.

Table 4.10: Results for Sample 4 obtained from Geant4 simulation.

Energy (MeV)	Geant4			
	Mass Attenuation Coefficient (cm^2/g)	LAC (1/cm)	HVL (cm)	MFP (cm)
0.01	9.6375	20.527875	0.03376614	0.04871425
0.02	9.3319	19.876947	0.03487191	0.05030954
0.03	9.9066	21.101058	0.03284893	0.04739099
0.04	9.077	19.33401	0.03585119	0.05172233
0.05	8.4565	18.012345	0.03848178	0.05551748
0.06	10.503	22.37139	0.03098364	0.04469995
0.081	9.1564	19.503132	0.0355403	0.05127382
0.112	8.1944	17.454072	0.03971263	0.05729322
0.122	7.8562	16.733706	0.04142222	0.05975963
0.136	7.4895	15.952635	0.04345033	0.06268557
0.161	8.5674	18.248562	0.03798366	0.05479884
0.223	14.264	30.38232	0.02281416	0.03291388
0.276	11.513	24.52269	0.02826554	0.04077856
0.302	11.025	23.48325	0.02951666	0.04258354
0.356	11.282	24.03066	0.02884428	0.04161351
0.384	13.41	28.5633	0.02426706	0.03500996
0.511	11.097	23.63661	0.02932515	0.04230725
0.662	8.5111	18.128643	0.03823492	0.05516133
0.835	10.569	22.51197	0.03079016	0.04442081
0.84	10.188	21.70044	0.03194162	0.04608201
1.17	8.0996	17.252148	0.04017744	0.0579638
1.275	9.6651	20.586663	0.03366972	0.04857514
1.333	12.054	25.67502	0.02699695	0.03894836
2	5.7214	12.186582	0.0568779	0.08205746
3	4.3771	9.323223	0.0743463	0.10725905
5	4.5399	9.669987	0.07168026	0.10341276
6	5.1187	10.902831	0.06357497	0.0917193
8	3.7958	8.085054	0.08573192	0.12368501
10	4.4353	9.447189	0.07337073	0.10585159
20	5.0673	10.793349	0.06421984	0.09264965

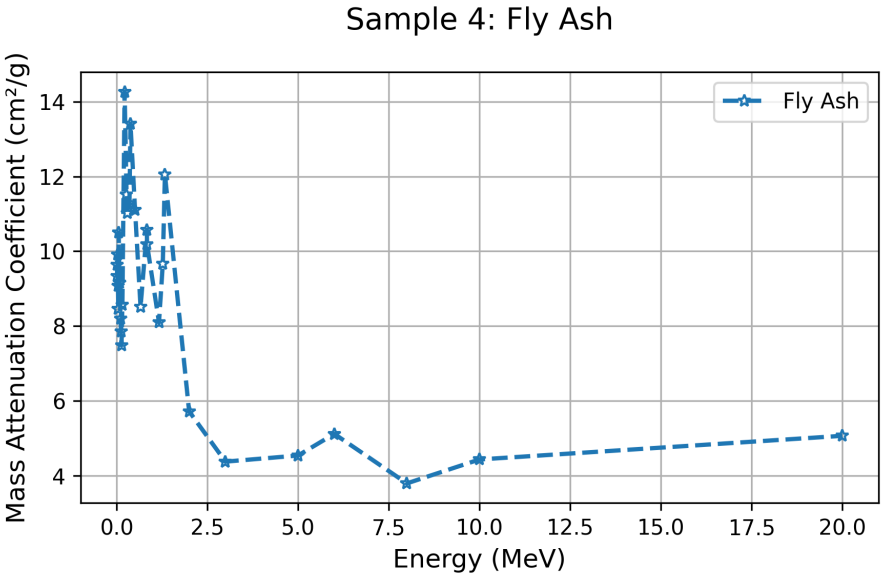

Figure 4.10: μ_m for Sample 4 simulated using Geant4.

Table 4.11: Results for Sample 5 obtained from Geant4 simulation.

Energy (MeV)	Geant4			
	Mass Attenuation Coefficient (cm^2/g)	LAC (1/cm)	HVL (cm)	MFP (cm)
0.01	9.6741	23.314581	0.0297302	0.04289161
0.02	9.1888	22.145008	0.03130038	0.0451569
0.03	9.7867	23.585947	0.02938814	0.04239813
0.04	8.6574	20.864334	0.03322163	0.04792868
0.05	8.3644	20.158204	0.03438536	0.04960759
0.06	10.626	25.60866	0.02706691	0.03904929
0.081	9.2519	22.297079	0.03108691	0.04484892
0.112	7.719	18.60279	0.03726039	0.05375538
0.122	7.9654	19.196614	0.03610778	0.05209252
0.136	7.313	17.62433	0.03932899	0.05673975
0.161	8.2105	19.787305	0.03502989	0.05053745
0.223	14.63	35.2583	0.01965912	0.02836212
0.276	11.679	28.14639	0.0246265	0.03552853
0.302	11.128	26.81848	0.02584588	0.03728772
0.356	11.212	27.02092	0.02565224	0.03700836
0.384	13.283	32.01203	0.02165271	0.03123826
0.511	10.961	26.41601	0.02623966	0.03785583
0.662	8.4613	20.391733	0.03399158	0.04903948
0.835	9.944	23.96504	0.02892326	0.04172745
0.84	10.177	24.52657	0.02826107	0.04077211
1.17	8.5992	20.724072	0.03344648	0.04825307
1.275	9.8576	23.756816	0.02917677	0.04209318
1.333	11.941	28.77781	0.02408617	0.034749
2	5.6858	13.702778	0.05058443	0.0729779
3	4.5536	10.974176	0.06316166	0.09112301
5	4.494	10.83054	0.06399932	0.0923315
6	5.2268	12.596588	0.05502658	0.07938658
8	3.9207	9.448887	0.07335755	0.10583257
10	4.0872	9.850152	0.07036919	0.10152128
20	5.0418	12.150738	0.05704569	0.08229953

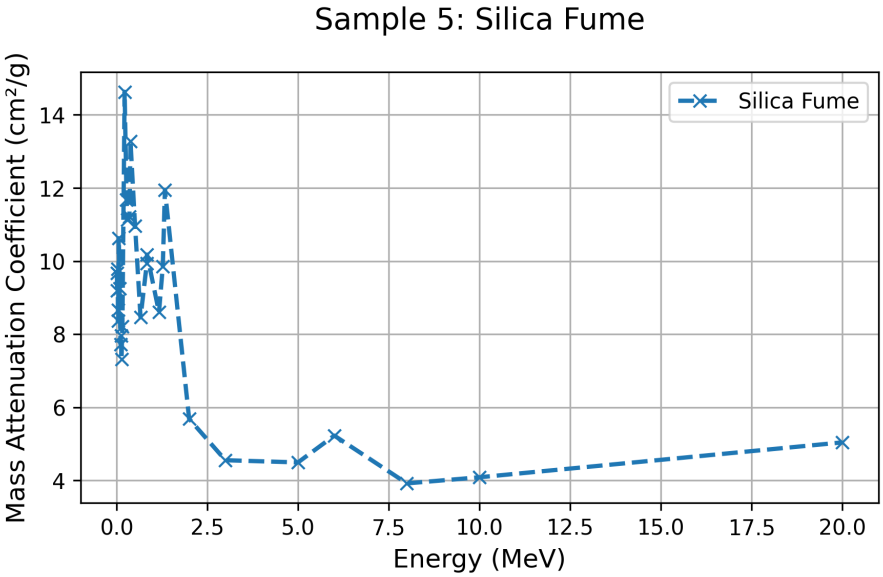

Figure 4.11: μ_m for Sample 5 simulated using Geant4.

4.2.2 Results Summary

The simulation results demonstrated a well-defined attenuation capability for neutron radiation across all evaluated cement-based samples over a wide energy range. Sample 3, which contained calcined calcium bentonite, exhibited the highest neutron attenuation strength, with the lowest half-value layer (HVL) and the highest linear attenuation coefficient (LAC) among all tested cementitious compounds. This superior shielding capability can be attributed to the composition and density of calcined calcium bentonite, which enhances neutron interactions.

The raw calcium bentonite cement sample, which ranked second after calcined calcium bentonite, displayed strong attenuation properties compared to the silica fume and fly ash composites. The Saudi cementitious materials demonstrated promising neutron shielding characteristics, making them potential candidates for alternative shielding applications in radiation protection.

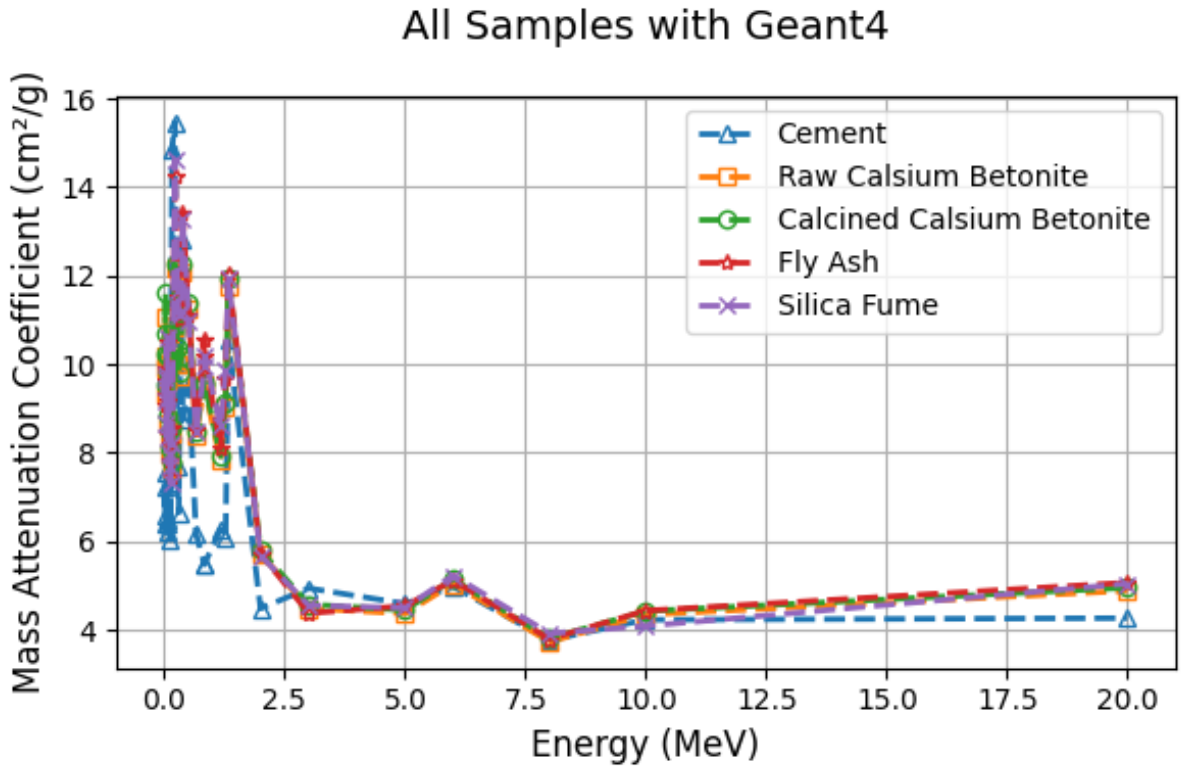

Figure 4.12: μ_m comparison for all five samples obtained by Geant4.

Chapter 5

Summary

5.1 Conclusions

This study investigated the radiation shielding properties of a new Saudi cement product using the Geant4 simulation toolkit and compared the results with EpiXS data. The findings demonstrated that the studied material exhibits significant attenuation capabilities for both gamma rays and neutrons, making it a promising alternative to conventional radiation shielding materials.

The Geant4 simulation results showed strong agreement with the reference values from EpiXS, with error margins remaining within acceptable limits. Additionally, the study highlighted that modifying the cement composition by incorporating certain additives can further enhance its shielding efficiency, making it more suitable for various engineering and industrial applications.

5.2 Recommendations

Based on the findings of this research, the following recommendations are proposed:

1. Expand the study scope to include other types of radiation, such as alpha and beta particles, to assess the material's performance across different radiation environments.
2. Conduct experimental validation to confirm the accuracy of the simulation results and enhance the reliability of the material's application in real-world scenarios.
3. Investigate the effect of additional high-density elements such as barium or tungsten in the cement mixture to further improve its shielding capabilities.
4. Explore potential applications of the material in nuclear and medical fields, particularly in designing protective shields for radiology rooms and nuclear laboratories.
5. Analyze long-term durability and environmental impact, including the effects of humidity and temperature, to ensure the material's sustainability and long-term effectiveness.

By implementing these recommendations, further advancements can be made in optimizing cement-based shielding materials for radiation protection applications.

Bibliography

[1] Hanan Akhdar and Rawan Alotaibi. "Geant4 Simulation of the Effect of Different Composites on Polyimide Photon and Neutron Shielding Properties". In: *Polymers* 15.8 (2023). ISSN: 2073-4360. DOI: 10.3390/polym15081973. URL: https://www.mdpi.com/2073-4360/15/8/1973.

[2] Muneerah A. Al-Aqeel. "Examining Low-Energy Gamma-Ray Protection of a New Promising Saudi Cement Product as Alternative Cementitious Material Using Geant4 Software". In: *Nuclear Technology* 0.0 (2024), pp. 1–13. DOI: 10.1080/00295450.2024.2355405. eprint: https://doi.org/10.1080/00295450.2024.2355405. URL: https://doi.org/10.1080/00295450.2024.2355405.

[3] Ya Yao et al. "Investigation of gamma ray shielding efficiency and mechanical performances of concrete shields containing bismuth oxide as an environmentally friendly additive". In: *Radiation Physics and Chemistry* 127 (2016), pp. 188–193. ISSN: 0969-806X. DOI: https://doi.org/10.1016/j.radphyschem.2016.06.028. URL: https://www.sciencedirect.com/science/article/pii/S0969806X16302031.

[4] Glen Knoll. *Radiation Detection and Measurement (4th ed.)* Hoboken, NJ: John Wiley, 2010. ISBN: 978-0-470-13148-0.

[5] Nicholas Tsoulfanidis and Sheldon Landsberger. *Measurement and Detection of Radiation*. 5th. CRC Press, 2021. DOI: 10.1201/9781003009849.

[6] Stephen Adjei et al. "Evaluation of calcined Saudi calcium bentonite as cement replacement in low-density oil-well cement system". In: *Journal of Petroleum Science and Engineering* 205 (2021), p. 108901. ISSN: 0920-4105. DOI: https://doi.org/10.1016/j.petrol.2021.108901. URL: https://www.sciencedirect.com/science/article/pii/S0920410521005623.